Mechanics and Mechanical Engineering
Vol. 22, No. 4 (2018) 1197–1221

https://doi.org/10.2478/mme-2018-0093

Exact Thermomechanical Analysis of Functionally Graded (FG) Thick-Walled Spheres

V. Yildirim
Department of Mechanical Engineering, University of Çukurova, Adana, Turkey
e-mail vebil@cu.edu.tr

Received (20 February 2018)
Revised (17 March 2018)
Accepted (20 November 2018)

The present study aims to provide a deeper understanding for the thermo-mechanical analysis of spheres made of non-homogeneous isotropic materials. To this end, Navier equations are solved analytically based on the spherically-symmetric plain-strain assumptions and closed-form formulas are proposed for the elastic fields in a simple-power-law graded spheres subjected to steady-state thermal and internal/external pressure loads. A comprehensive parametric study is then performed with both functionally-graded hypothetical and physical materials. Two benchmark examples are reconsidered with hypothetically chosen inhomogeneity indexes. Effects of inhomogeneity indexes are reviewed in these examples. Differently from the literature, thickness effects are also examined under separate and combined loads together with the thermo-mechanical behavioral differences in spheres and cylinders. Finally three physical metal-ceramic pairs are studied originally with appropriate inhomogeneity indexes which are defined as the inner surface is full ceramic and the outer surface is full metal. Results are presented in graphical and tabular forms.

Keywords: Thermo-mechanical, exact elasticity solution, functionally graded, thick-walled sphere, thickness effect.

1. Introduction

Elasticity solutions for spheres were first found for isotropic and homogeneous linear elastic materials. Timoshenko and Goodier [1] obtained analytical expressions of stresses and displacement in a thick-walled sphere subjected to internal and external pressure. Borisov [1] analytically worked on the stress and deformation distribution in a system of thick-walled spheres made of a homogeneous and isotropic material under external pressure. Gamer [3], Megahed [4], and Gao [5] studied the elastic-plastic behavior of spherical shells.

Yildirim [6] proposed closed-form analytical formulas for heat-induced, internal/external pressure-induced, and centrifugal force-induced axisymmetric elastic fields in a thick-walled spherical vessel, a cylindrical vessel, and a uniform disc at a

specified constant surface temperature and at a constant angular velocity by considering isotropic and homogeneous linear elastic materials. As it is well known, the discovery of functionally graded materials (FGM) in Japan dates back to the late 1980s. FGMs are made of a mixture with arbitrary composition of at least two different materials, and so the overall material properties may be spatially and continuously distributed along the preferred directions as desired. In this respect, FGMs are assumed to be an alternative to the laminated composites due to its outstanding thermal and mechanical features.

Studies on the elastic behavior of structures made of FGMs have been gained considerable attention by the scholars 1980 and thereafter. Most of these studies have been directed towards the structures subjected to mechanical loads. Among these, Chen [7] exactly investigated the stress distribution in a rotating, spherically isotropic, FGM spherical shell that has its elastic constants and mass density as functions of the radial coordinate. Güven and Baykara [8] considered a FGM hollow sphere with spherical isotropy subjected to internal pressure in the framework of linear isotropic elasticity. You et al. [9] presented an accurate method to carry out elastic analysis of thick-walled spherical pressure vessels subjected to internal pressure. Two kinds of pressure vessel were considered there, one consists of two homogeneous layers near the inner and outer surfaces of the vessel and one exponentially graded layer in the middle; the other consists of the functionally graded material only.

Chen and Lin [10] carried out a numerical elastic analysis for a thick cylinder/sphere made of exponentially graded materials. Tutuncu and Temel [11] worked on the axisymmetric displacements and stresses in FGM hollow cylinders, disks and spheres subjected to uniform internal pressure by using Complementary Functions method. Li et al. [12] studied pressurized hollow spherical vessels with arbitrary radial non-homogeneity with the help of Fredholm integrals. Saidi et al. [13] proposed exact solutions for the displacement and stresses in a thick-walled linearly and exponentially graded spherical vessels under internal and external pressures.

Chen and Lin [14] examined analytically the elastic behavior of thick-walled, single or multi-layered, and arbitrarily graded cylinders/spheres with the help of the method of transmission matrix. They also presented a lot of numerical examples. For linear elastic hollow cylinders and spheres, Nie et al. [15] presented a technique to tailor materials which are graded by a radially varying volume fraction rule to attain through-the-thickness either a constant circumferential stress or a constant in-plane shear stress. Nejad et al. [16] derived exact closed-form solutions for stresses and the displacements in thick spherical shells made of FGMs with exponential-varying properties subjected to internal and external pressure. A finite element method was also used for comparison aims. Ghannad and Nejad [17] presented a complete analytical solution for power-law graded thick-walled spherical shells subjected to internal and/or external pressures. They compared the solution with finite element method.

Karami et al. [18] analytically determined the displacement and stress components in a thick-walled spherical pressure vessels made of parabolically graded materials subjected to internal and external pressure. They showed that their results and the solutions carried out through the ANSYS had a good agreement. Nejad et al. [19] used a semi-analytical iterative method for the elastic analysis of thick-

walled spherical pressure vessels made of exponentially graded materials subjected to internal pressure. A numerical solution, using finite element method (FEM), was also presented.

Anani and Rahimi [20] used a member of Ericksen's family of universal solutions to analytically investigate radial expansion/contraction of a sphere made of isotropic and inhomogeneous hyperelastic material under internal and external pressures. Hyperelastic behavior was modeled by using modified neo Hookean strain energy function with power-law graded material. Shrivastava et al. [21] studied the elastic analysis of rotating spherical pressure vessels made of Mori-Tanaka scheme graded aluminum and zirconia materials by finite element method based on principle of stationary total potential.

Some researchers devoted their effort to work on steady state or transient thermal analyses of spheres. From those, Norouzi et al. [22] presented as the first time an exact analytical solution for steady conductive heat transfer in multilayer spherical fiber reinforced composite laminates under the general linear boundary conditions that are suitable for various conditions including combinations of conduction, convection, and radiation both inside and outside of the sphere. The separation of variables were used by solving the set of equations related to the coefficient of Fourier–Legendre series of temperature distribution using the recursive Thomas algorithm.

Singh et al. [23] and Jain et al. [24] proposed an analytical series solution for transient heat conduction in $r - \theta$ spherical coordinates for the heat conduction of spherical isotropic multi-layered materials under different kind of boundary conditions. Lu and Viljanen [25] proposed an analytical method which is free of eigenvalue and residue calculations to solve the equation of heat conduction in a layered sphere subject to a time-dependent boundary temperature. Yildrim [26] conducted analytically thermal analyses of radially functionally simple power-law graded thick-walled a spherical vessel and an infinite cylindrical vessel or a circular annulus by the steady-state 1-D Fourier heat conduction theory under Dirichlet's boundary conditions.

Some of scholar addressed just thermal stresses and displacements in spherical vessels. Cheung et al. [27] and Takeuti and Tanigawa [28] considered transient thermal stresses in spheres. Based on the perturbation method Obata and Noda [29] studied one-dimensional steady thermal stresses in a functionally graded circular hollow cylinder and a hollow sphere. The analytical solution for the thermal stresses in spheres made of functionally graded materials were given by Lutz and Zimmerman [30]. By employing an analytical–numerical technique, Tsai et al. [31] investigated the non-Fourier effects on the dynamic thermal behavior of spherical media, including solid, hollow and bi-layered composite spheres, due to sudden temperature changes on the surfaces. Bagri and Eslami [32] proposed a new unified formulation for the generalized theories of the coupled thermoelasticity based on the Lord–Shulman, Green–Lindsay, and Green–Naghdi models for the anisotropic heterogeneous materials.

After 2000s, the spheres under combined mechanical and thermal loads have been got going to be considered. Foremost among these, Eslami et al. [33] proposed a general benchmark solution for the one-dimensional steady-state thermal and mechanical stresses in a hollow thick power-law graded sphere. Poultangari et

al. [34] developed an analytical method based on the Legendre polynomials to obtain the solution for the two-dimensional steady state thermal and mechanical stresses in a hollow power-law graded thick sphere.

Alavi et al. [35] presented a FEM analysis to study the thermoelastic behavior of thick functionally graded hollow sphere under thermal and mechanical loads. The rule of mixture and Mori-Tanaka schemes are both used to estimate the effective mechanical properties of FG sphere. Solution of the heat conduction equation and the Navier equation were obtained by using the Galerkin finite element method and by generating 100 elements along the radial direction of FG sphere. Based on the eigen function's Fourier expansion, Jabbari et al. [36] considered analytically the classic coupled thermoelasticity model of hollow and solid spheres under radial-symmetric loading condition. In their study, the thermal and mechanical boundary conditions, the body force, and the heat source were considered in the most general forms, where no limiting assumption was used. This generality allowed to simulate a variety of applicable problems.

Nayak et al. [37] determined analytically the displacements, strains, and stresses of a power-law graded thick spherical vessel under the third kind thermal boundary conditions, with steady-state unidirectional radial heat conduction and general mechanical boundary conditions. Jabbari et al. [38] presented a general solution for the one-dimensional steady-state thermal and mechanical stresses in a hollow thick sphere made of porous power-law graded material. Bayat et al. [39] carried out a thermo-mechanical analysis of a power-law graded hollow sphere subjected to pressure and one-dimensional steady-state thermal loads. They offered analytical solutions for both values of inhomogeneity index of the thermal conductivity, $\beta = -1$ and $\beta \neq -1$. They investigated the effects of hypothetically chosen inhomogeneity indexes of $\beta = -2,\ -1,\ 0,\ 1,\ 2$ which were all assumed to be equal to each other on the elastic fields of the sphere under separate and combined internal pressure and thermal loads. They also used a FEM solution to validate their results by presenting some numerical data for $\beta = 1$ and $\beta = -1$.

Functions which are used for material grading may differ with respect to the requirements. For some types of those functions such as a simple power, an exponential, and a linear variation, it is possible to obtain a closed form solution to the problem. For instance if the grading function is chosen as a common simple power rule as in the present study, the governing differential equation called Navier equation turns into a second order Euler-Cauchy type differential equation with constant coefficients. For linearly varying properties, the solution is obtained in terms of hyper-geometric functions. If the material grading is performed by an exponential function then Whittaker/Kumer functions or Frobenius series are employed in the solution. However, in general, for other types of grading rules it is required to use a numerical solution techniques.

In the literature, especially analytical studies on such structures subjected to the only the inner pressure are relatively large. The number of studies considering the simultaneous effects of both the inner and outer pressures are scarce. The present study deals with those effects both separately and simultaneously for spheres made of power-law graded physical and hypothetic materials.

In the present study, at a first place, Navier equations for the linear elastic behavior of a sphere subjected to steady-state thermal loads under prescribed sur-

face temperatures and internal/external pressure loads are derived based on the spherically symmetric plain strain assumptions. Those equations are then solved analytically with the help of Euler-Cauchy equations. To validate the present results, two benchmark examples are reconsidered with hypothetically chosen inhomogeneity indexes of $\beta = -3, -2, -1, 0, 1, 2, 3$. The investigation of the thickness effect is also included in these examples. Apart from those a comparison of equivalent stresses between a spherical and cylindrical structure having the same required dimensions and loading is made. Finally, three types of physical metal-ceramic pairs namely nickel-silicon nitride (Ni-Si_3N_4), aluminum-aluminum oxide (Al-Al_2O_3), and stainless steel-zirconium oxide ($SUS304$-ZrO_2), are studied with appropriate inhomogeneity indexes. It is assumed that elasticity modulus, thermal expansion coefficient and thermal conductivity are all to be continuously changed in the radial direction with different inhomogeneity indexes. Those inhomogeneity indexes are determined as the inner surface is to be full ceramic and the outer surface is to be full metal. The intermediate surfaces consist of the mixture of a metal and a ceramic which obeys the power law gradient. Poisson's ratio is assumed to be unchanged along the radial coordinate. The graphs of examples with physical materials comprise FGM sphere as well as only metal and only ceramic spheres. It may be noted that results for an isotropic and homogeneous materials are computed directly by using formulas in References [6, 26] to allow an auto-control of FGM results (see Appendices A and B).

2. Derivation of Navier Equation

Let's consider a thick-walled sphere of inside radius a, and outside radius b (Fig. 1). The radial, tangential, and azimuthal coordinates are denoted by r, θ, and φ. Let's use the prime symbol for the derivative with respect to the radial coordinate in the following derivations.

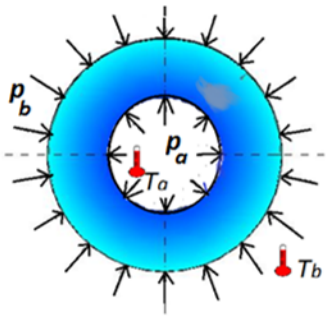

Figure 1 Characteristic section of a spherically symmetric structure

Denoting the radial displacement by u_r, the unit radial strain by ε_r, and the unit tangential strain by ε_θ, the strain-displacement relations for spheres are as follows under spherically symmetric plane-strain and small displacements assumptions.

$$\varepsilon_r(r) = u_r'(r), \qquad \varepsilon_\theta(r) = \varepsilon_\varphi(r) = \frac{u_r(r)}{r}\,. \tag{1}$$

For a linearly elastic, isotropic but non homogeneous material the stress-strain relations are to be

$$\begin{aligned}\sigma_r(r) &= C_{11}(r)\varepsilon_r(r) + 2C_{12}(r)\varepsilon_\theta(r) - (C_{11}(r) + 2C_{12}(r))\,\alpha(r)T(r)\\ \sigma_\theta(r) &= C_{12}(r)\varepsilon_r(r) + (C_{11}(r) + C_{12}(r))\,\varepsilon_\theta(r) - (C_{11}(r) + 2C_{12}(r))\,\alpha(r)T(r)\,,\end{aligned} \quad (2)$$

where σ_r is the radial stress, σ_θ is the hoop stress, α is the thermal expansion coefficient, $T(r)$ is the temperature distribution along the radial coordinate, and C_{ij} are

$$C_{11}(r) = \frac{(1-\nu)}{(1+\nu)(1-2\nu)}E(r), \quad C_{12}(r) = \frac{\nu}{(1+\nu)(1-2\nu)}E(r) \quad (3)$$

In the above, ν is the Poisson's ratio. If Eq. (1) is substituted into Eq. (2) by defining the following

$$\lambda = \frac{C_{12}(r)}{C_{11}(r)} = \frac{\nu}{1-\nu} \quad (4)$$

Hooke's law is in the form of

$$\begin{aligned}\sigma_r(r) &= C_{11}(r)u_r'(r) + 2\lambda C_{11}(r)\frac{u_r(r)}{r} - (1+2\lambda)C_{11}(r)\alpha(r)T(r)\,,\\ \sigma_\theta(r) &= \lambda C_{11}(r)u_r'(r) + (1+\lambda)C_{11}(r)\frac{u_r(r)}{r} - (1+2\lambda)C_{11}(r)\alpha(r)T(r)\,.\end{aligned} \quad (5)$$

The equilibrium equation in the radial direction in the absence of the body forces is

$$\frac{1}{r^2}\left(r^2\sigma_r(r)\right)' - \frac{2}{r}\sigma_\theta(r) = \sigma_r'(r) + \frac{2}{r}\left(\sigma_r(r) - \sigma_\theta(r)\right) = 0\,. \quad (6)$$

If the equilibrium equation is rewritten by considering Eq. (5), Navier equation for thermo-mechanical analysis of a sphere made of an arbitrarily graded material is derived as follows

$$\begin{pmatrix} \left(-\frac{2}{r^2} + \frac{2}{r}\lambda\frac{C_{11}'(r)}{C_{11}(r)}\right)u_r(r) \\ +\left(\frac{2}{r} + \frac{C_{11}'(r)}{C_{11}(r)}\right)u_r'(r) + u_r''(r) \end{pmatrix} = \begin{pmatrix} \left(\alpha(r)\frac{C_{11}'(r)}{C_{11}(r)} + \alpha'(r)\right)(1+2\lambda)T(r) \\ +(1+2\lambda)\alpha(r)T'(r) \end{pmatrix} \quad (7)$$

This is a second order differential equation with variable coefficients. To get an analytical solution to the problem, the material grading may be assumed to obey the following simple power rule.

$$E(r) = E_a(\frac{r}{a})^\beta\,, \quad \alpha(r) = \alpha_a(\frac{r}{a})^n\,, \quad k(r) = k_a(\frac{r}{a})^\mu\,. \quad (8)$$

Substitution of the above in Eq. (7) gives

$$\begin{aligned}&\frac{2(-1+\beta\lambda)}{r^2}u_r(r) + \frac{2+\beta}{r}u_r'(r) + u_r''(r) =\\ &\begin{pmatrix} \left(\frac{\beta}{r}\alpha_a\left(\frac{r}{a}\right)^n + \frac{n}{a}\alpha_a\left(\frac{r}{a}\right)^{n-1}\right)(1+2\lambda)T(r) \\ +(1+2\lambda)\alpha_a(\frac{r}{a})^nT'(r) \end{pmatrix}\end{aligned} \quad (9)$$

To complete the derivation, the determination of the temperature distribution along the thickness which is govern by the following

$$\frac{1}{r^2}\frac{d}{dr}\left(r^2 k(r)\frac{dT(r)}{dr}\right)=0 \tag{10}$$

is required. In Eq. (10) $k\,(r)$ stands for the thermal conductivity. For any arbitrary material grading rule this equation becomes

$$\left(\frac{2}{r}+\frac{k'(r)}{k(r)}\right)T'(r)+T''(r)=0 \tag{11}$$

If the power-law grading rule in Eq. (8) is employed, the above turns to the following

$$\frac{2+\mu}{r}T'(r)+T''(r)=0 \tag{12}$$

Yildirim [6] solved Eq. (12) under boundary conditions, $T(a)=T_a$ and $T(b)=T_b$, as follows

$$T(r)=\frac{r^{-1-\mu}\left(\begin{array}{l}-b^{1+\mu}r^{1+\mu}T_b\\ +a^{1+\mu}(r^{1+\mu}T_a+b^{1+\mu}(-T_a+T_b))\end{array}\right)}{a^{1+\mu}-b^{1+\mu}}=\ \phi_1+\ \phi_2 r^{-1-\mu} \tag{13}$$

where

$$\phi_1=\frac{a^{1+\mu}T_a-T_b b^{1+\mu}}{a^{1+\mu}-b^{1+\mu}},\quad \phi_2=\frac{a^{1+\mu}b^{1+\mu}(T_b-T_a)}{a^{1+\mu}-b^{1+\mu}} \tag{14}$$

In the solution given by Eq. (13), when $\mu=-1$, $T\,(r)$ becomes indefinite [6]. As stated above, Bayat et al. [39] also considered this situation in their derivations. However this problem is easily numerically taken care of by using real numbers instead integers for the inhomogeneity index of the thermal conductivity [6], say μ= −1.000000001. Solution of Eq. (12) for isotropic and homogeneous materials is also given in Appendix A. If the solution in Eq. (13) is implemented in Eq. (9) one gets

$$\begin{array}{l}\frac{2}{r^2}(-1+\beta\lambda)u_r(r)+\frac{1}{r}(2+\beta)u_r'(r)+u_r''(r)=\\ (a^{-n}r^{-2+n-\mu}\alpha_a(n+\beta)(1+2\lambda)(r^{1+\mu}\phi_1+\phi_2))+\\ (-a^{-n}r^{-2+n-\mu}\alpha_a(1+2\lambda)(1+\mu)\phi_2)=\\ a^{-n}r^{-2+n-\mu}\alpha_a(1+2\lambda)(r^{1+\mu}(n+\beta)\phi_1+(-1+n+\beta-\mu)\phi_2)\end{array} \tag{15}$$

The above Navier equation may be simplified as follows

$$\frac{2(-1+\beta\lambda)}{r^2}u_r(r)+\frac{(2+\beta)}{r}u_r'(r)+u_r''(r)=r^{-2+n-\mu}\Delta_1(r^{1+\mu}\Delta_2+\Delta_3)\,, \tag{16}$$

by introducing the following constants

$$\Delta_1=a^{-n}\alpha_a(1+2\lambda),\quad \Delta_2=(n+\beta)\phi_1,\quad \Delta_3=(-1+n+\beta-\mu)\phi_2\,. \tag{17}$$

Equation (16), a second order nonhomogeneous differential equation with constant coefficients, now may be solved by employing Cauchy-Euler equation. It may be noted that Poisson's ratio is assumed to remain constant along the radial coordinate in the derivation given above. The arithmetic mean of Poisson's ratios of metal and ceramic is used in the examples.

3. Solution of Navier Equation under Internal/External Pressures

Homogeneous solution of the Navier equation in Eq. (16)

$$\frac{2(-1+\beta\lambda)}{r^2}u_r(r)+\frac{(2+\beta)}{r}u_r'(r)+u_r''(r)=0 \tag{18}$$

under boundary conditions, $\sigma_r(a)=-p_a$ and $\sigma_r(b)=-p_b$, offers the elastic field due to both internal and external pressures, p_a and p_b, as follows

$$\begin{aligned} u_r(r) &= r^{\frac{1}{2}(-1-\beta-\xi)}(A_1+A_2r^{\xi}) \\ \sigma_r(r) &= -\frac{1}{2}C_{11}(r)r^{\frac{1}{2}(-3-\beta-\xi)}\begin{pmatrix} A_1(1+\beta-4\lambda+\xi) \\ +A_2r^{\xi}(1+\beta-4\lambda-\xi)\end{pmatrix} \\ \sigma_\theta(r) &= \frac{1}{2}C_{11}(r)r^{\frac{1}{2}(-3-\beta-\xi)}\begin{pmatrix} A_1(2-\lambda(-1+\beta+\xi)) \\ +A_2r^{\xi}(2+\lambda(1-\beta+\xi))\end{pmatrix}\end{aligned} \tag{19}$$

where

$$\begin{aligned} \xi &= \sqrt{9+2\beta+\beta^2-8\beta\lambda} \\ C_{11}(r) &= \frac{a^{-\beta}E_ar^{\beta}(1-\nu)}{(1-2\nu)(1+\nu)} \\ A_1 &= \frac{2(2\nu^2+\nu-1)a^{\frac{\beta+\xi}{2}}b^{\frac{\xi-\beta}{2}}(b^{3/2}p_ba^{\frac{\beta+\xi}{2}}-a^{3/2}p_ab^{\frac{\beta+\xi}{2}})}{E_a(\nu-1)(a^{\xi}-b^{\xi})(\beta-4\lambda+\xi+1)} \\ A_2 &= \frac{2(2\nu^2+\nu-1)a^{\beta/2}b^{-\beta/2}(b^{\beta/2}p_aa^{\frac{\xi+3}{2}}-a^{\beta/2}p_bb^{\frac{\xi+3}{2}})}{E_a(\nu-1)(a^{\xi}-b^{\xi})(\beta-4\lambda-\xi+1)}\end{aligned} \tag{20}$$

Explicit forms of solution (19) are to be

$$\begin{aligned} u_r(r) &= -\frac{2p_a(2\nu^2+\nu-1)a^{\frac{1}{2}(\beta+\xi+3)}r^{\frac{1}{2}(-\beta-\xi-1)}(b^{\xi}(\beta-4\lambda-\xi+1)-r^{\xi}(\beta-4\lambda+\xi+1))}{E_a(\nu-1)(a^{\xi}-b^{\xi})(\beta-4\lambda-\xi+1)(\beta-4\lambda+\xi+1)} \\ &\quad -\frac{2p_b(2\nu^2+\nu-1)a^{\beta}b^{\frac{1}{2}(-\beta+\xi+3)}r^{\frac{1}{2}(-\beta-\xi-1)}(a^{\xi}(\beta-4\lambda-\xi+1)-r^{\xi}(\beta-4\lambda+\xi+1))}{E_a(\nu-1)(a^{\xi}-b^{\xi})(\beta-4\lambda+\xi+1)(-\beta+4\lambda+\xi-1)} \\ \sigma_r(r) &= \frac{p_aa^{\frac{1}{2}(-\beta+\xi+3)}(b^{\xi}-r^{\xi})r^{\frac{1}{2}(\beta-\xi-3)}}{(a^{\xi}-b^{\xi})}+\frac{p_bb^{\frac{1}{2}(-\beta+\xi+3)}(a^{\xi}-r^{\xi})r^{\frac{1}{2}(\beta-\xi-3)}}{(b^{\xi}-a^{\xi})} \\ \sigma_\theta(r) &= \\ &\frac{p_aa^{\frac{1}{2}(-\beta+\xi+3)}r^{\frac{1}{2}(\beta-\xi-3)}}{(a^{\xi}-b^{\xi})(\beta-4\lambda-\xi+1)(\beta-4\lambda+\xi+1)}\begin{pmatrix} b^{\xi}(\beta-4\lambda-\xi+1)(\lambda(\beta+\xi-1)-2) \\ +r^{\xi}(\beta-4\lambda+\xi+1)(\lambda(-\beta+\xi+1)+2)\end{pmatrix} \\ &+\frac{p_bb^{\frac{1}{2}(-\beta+\xi+3)}r^{\frac{1}{2}(\beta-\xi-3)}}{(a^{\xi}-b^{\xi})(\beta-4\lambda+\xi+1)(-\beta+4\lambda+\xi-1)}\begin{pmatrix} a^{\xi}(\beta-4\lambda-\xi+1)(\lambda(\beta+\xi-1)-2) \\ +r^{\xi}(\beta-4\lambda+\xi+1)(\lambda(-\beta+\xi+1)+2)\end{pmatrix}\end{aligned} \tag{21}$$

4. Solution of Navier Equation under Prescribed Surface Temperatures

The radial displacement is obtained from the general solution of Eq. (16) under boundary conditions, $\sigma_r(a)=0$ and $\sigma_r(b)=0$, as follows

$$\begin{aligned} u_r(r) &= r^n\Delta_1\left(\frac{r\Delta_2}{\beta+n(3+n+\beta)+2\beta\lambda}+\frac{r^{-\mu}\Delta_3}{-2+n+n^2+n\beta+2\beta\lambda-(1+2n+\beta)\mu+\mu^2}\right) \\ &\quad + r^{\frac{1}{2}(-1-\beta-\xi)}C_1+r^{\frac{1}{2}(-1-\beta+\xi)}C_2\end{aligned} \tag{22}$$

By introducing the new constants

$$\Delta_4 = \frac{\Delta_1\Delta_2}{\beta + n(3+n+\beta) + 2\beta\lambda}$$
$$\Delta_5 = \frac{\Delta_1\Delta_3}{-2+n+n^2+n\beta+2\beta\lambda-(1+2n+\beta)\mu+\mu^2} \tag{23}$$

eq. (24) and stresses take the following form

$$u_r(r) = r^{\frac{1}{2}(-1-\beta-\xi)}C_1 + r^{\frac{1}{2}(-1-\beta+\xi)}C_2 + r^{1+n}\Delta_4 + r^{n-\mu}\Delta_5 \quad (a)$$
$$\sigma_r(r) =$$
$$-\frac{1}{2}a^{-n}C_{11}(r)r^{\frac{1}{2}(-3-\beta-2\mu-\xi)}\begin{pmatrix} a^n(C_1r^\mu(1+\beta-4\lambda+\xi) \\ -r^{\xi/2}(2r^{\frac{1}{2}(1+2n+\beta)}(r^{1+\mu}\Delta_4(1+n+2\lambda) \\ +\Delta_5(n+2\lambda-\mu)) + C_2r^{\mu+\frac{\xi}{2}}(-1-\beta+4\lambda+\xi))) \\ +2r^{\frac{1}{2}(1+2n+\beta+\xi)}\alpha_a(1+2\lambda)(r^{1+\mu}\phi_1+\phi_2) \end{pmatrix} \quad (b)$$
$$\sigma_\theta(r) =$$
$$\frac{1}{2}C_{11}(r)r^{\frac{1}{2}(-3-\beta)}\begin{pmatrix} C_1r^{-\xi/2}(2-\lambda(-1+\beta+\xi)) \\ +a^{-n}r^{-\mu}(a^n(2r^{\frac{1}{2}(1+2n+\beta)}(\Delta_5+r^{1+\mu}\Delta_4(1+(2+n)\lambda) \\ +\Delta_5\lambda(1+n-\mu)) + C_2r^{\mu+\frac{\xi}{2}}(2+\lambda-\beta\lambda+\lambda\xi)) \\ -2r^{\frac{1}{2}(1+2n+\beta)}\alpha_a(1+2\lambda)(r^{1+\mu}\phi_1+\phi_2)) \end{pmatrix} \quad (c)$$
(24)

where

$$C_1 = \frac{2b^{\frac{1}{2}(\xi-2\mu)}a^{\frac{1}{2}(\xi-2(\mu+n))}}{(a^\xi-b^\xi)(\beta-4\lambda+\xi+1)}$$
$$\begin{pmatrix} -\alpha_a(2\lambda+1)a^{\mu+\frac{\xi}{2}}b^{\frac{1}{2}(\beta+2n+1)}(\phi_1b^{\mu+1}+\phi_2) \\ +\alpha_a(2\lambda+1)\phi_1b^{\mu+\frac{\xi}{2}}a^{\frac{\beta+3}{2}+\mu+n} + \alpha_a(2\lambda+1)\phi_2a^{\frac{1}{2}(\beta+2n+1)}b^{\mu+\frac{\xi}{2}} \\ +b^{\frac{1}{2}(\beta+2n+1)}a^{\mu+n+\frac{\xi}{2}}(\Delta_4b^{\mu+1}(2\lambda+n+1)+\Delta_5(2\lambda-\mu+n)) \\ -\Delta_4(2\lambda+n+1)b^{\mu+\frac{\xi}{2}}a^{\frac{\beta+3}{2}+\mu+2n} - \Delta_5a^{\frac{1}{2}(\beta+4n+1)}b^{\mu+\frac{\xi}{2}}(2\lambda-\mu+n) \end{pmatrix} (a) \quad (25)$$

$$C_2 = -\frac{2b^{-\mu}a^{-\mu-n}}{(a^\xi-b^\xi)(-\beta+4\lambda+\xi-1)}$$
$$\begin{pmatrix} -a^{-\mu+n}b^{\frac{1}{2}(\beta+2n+\xi+1)}(\Delta_4b^{\mu+1}(2\lambda+n+1)+\Delta_5(2\lambda-\mu+n)) \\ -\alpha_a(2\lambda+1)\phi_1b^\mu a^{\frac{1}{2}(\beta+2\mu+2n+\xi+3)} \\ -\alpha_a(2\lambda+1)\phi_2b^\mu a^{\frac{1}{2}(\beta+2n+\xi+1)} \\ +\Delta_4b^\mu(2\lambda+n+1)a^{\frac{1}{2}(\beta+2\mu+4n+\xi+3)} \\ +\Delta_5b^\mu(2\lambda-\mu+n)a^{\frac{1}{2}(\beta+4n+\xi+1)} \\ +\alpha_a(2\lambda+1)a^\mu(\phi_1b^{\mu+1}+\phi_2)b^{\frac{1}{2}(\beta+2n+\xi+1)} \end{pmatrix} (b) \quad (26)$$

5. Validation of the Results

By assuming that all the homogeneity indexes are to be the same, $\beta = n = \mu$, Jabbari et al. [40] used the following material and geometrical properties to study the thermo-mechanical analysis of the cylinders subjected to both internal pressure and surface temperature differences: $a = 1.0\,\mathrm{m}$; $b = 1.2\,\mathrm{m}$; $\beta = -2, -1, 0, 1, 2$; $\nu = 0.3$; $E_a = 200\,\mathrm{GPa}$, $p_a = 50\,\mathrm{MPa}$; $p_b = 0$; $\alpha_a = 1.2 \cdot 10^{-6}$ $1/^\circ\,\mathrm{C}$; $T_a = 10^\circ\,\mathrm{C}$; $T_b = 0^\circ\,\mathrm{C}$.

Eslami et al. [33] also used the same data for the same analysis of spheres with $\beta = -2, -1, 0, 1, 2, 3$. They presented the combined results in only graphical form.

Table 1 Variation of the dimensionless radial displacement with the inhomogeneity index under separate and combined loads for the first test example [33]

$u_r/a \times 10^{-6}$							
r/a	$\beta=-3$	$\beta=-2$	$\beta=-1$	$\beta=0$	$\beta=1$	$\beta=2$	$\beta=3$
Heat induced							
1.	5.41101	5.3678	5.3223	5.27473	5.22512	5.17368	5.12059
1.04	5.97455	5.94041	5.90376	5.8648	5.82354	5.78018	5.73488
1.08	6.29515	6.27851	6.25919	6.23729	6.21281	6.18585	6.15655
1.12	6.42566	6.42712	6.42614	6.42273	6.41681	6.40844	6.39765
1.16	6.40819	6.4229	6.43566	6.44645	6.45515	6.46173	6.4662
1.2	6.27646	6.29583	6.31358	6.32967	6.34397	6.35646	6.36711
Pressure induced							
1.	0.0006717	0.0006196	0.0005700	0.0005231	0.00047876	0.00043708	0.00039802
1.04	0.0006430	0.0005927	0.0005448	0.0004995	0.00045668	0.00041644	0.00037873
1.08	0.0006177	0.0005690	0.0005228	0.0004790	0.00043774	0.00039890	0.00036253
1.12	0.0005953	0.0005483	0.0005036	0.0004613	0.00042144	0.00038393	0.00034880
1.16	0.0005757	0.0005302	0.0004869	0.0004460	0.00040738	0.00037108	0.00033710
1.2	0.0005585	0.0005144	0.0004724	0.0004327	0.00039523	0.00036001	0.00032703
(Heat + Pressure) induced							
1.	0.0006771	0.0006249	0.0005753	0.0005284	0.00048399	0.00044225	0.00040314
1.04	0.0006490	0.0005986	0.0005507	0.0005053	0.00046250	0.00042222	0.00038446
1.08	0.0006239	0.0005753	0.0005291	0.0004853	0.00044395	0.00040509	0.00036868
1.12	0.0006017	0.0005547	0.0005101	0.0004678	0.00042785	0.00039034	0.00035520
1.16	0.0005821	0.0005366	0.0004934	0.0004524	0.00041383	0.00037755	0.00034356
1.2	0.0005648	0.0005207	0.0004787	0.0004390	0.00040157	0.00036637	0.00033340

This example is chosen as the first test example in the present work. Fig. 2 shows elastic fields under separate and combined internal pressure and thermal loads for this first test example. It is revealed that the graphs for combined effects in Fig. 2 are in compliance with Eslami et al.'s graphs [33]. For the example considered, Fig. 2 suggests that effects of the thermal loads are almost negligible since the surface temperature difference was taken as relatively small. For this example some numerical data for displacements and stresses are presented in Tables 1–2. In Tab. 2, equivalent von Mises stress is defined by

$$\sigma_{eq}(r) = \sqrt{2}\,|\sigma_r(r) - \sigma_\theta(r)| \tag{27}$$

For a sphere in the first test example, from Tab. 2, β= 3 may be assumed as a better inhomogeneity index by offering almost uniform radial distribution.

Table 2 Variation of the dimensionless radial stress, hoop stress and equivalent stress with the inhomogeneity index under separate and combined loads for the first test example [33]

r/a	$\beta=-3$	$\beta=-2$	$\beta=-1$	$\beta=0$	$\beta=1$	$\beta=2$	$\beta=3$
σ_r/p_a							
Heat induced							
1.	0.	0.	0.	0.	0.	0.	0.
1.04	-0.001954	-0.002047	-0.002144	-0.002243	-0.002345	-0.0024501	-0.002558
1.08	-0.002399	-0.002610	-0.002848	-0.003080	-0.0033395	-0.0036158	-0.003910
1.12	-0.001981	-0.002234	-0.002526	-0.002830	-0.0031799	-0.0035652	-0.003994
1.16	-0.001010	-0.001282	-0.001494	-0.001740	-0.0020218	-0.0023484	-0.002725
1.20	0.	0.	0.	0.	0.	0.	0.
Pressure induced							
1.	-1.	-1.	-1.	-1.	-1.	-1.	-1.
1.04	-0.689617	-0.705642	-0.721292	-0.736519	-0.751275	-0.765518	-0.779213
1.08	-0.449482	-0.469856	-0.490267	-0.510635	-0.530876	-0.550909	-0.570654
1.12	-0.262365	-0.279762	-0.297619	-0.315874	-0.334459	-0.353302	-0.37233
1.16	-0.11565	-0.125623	-0.136098	-0.147056	-0.158474	-0.170325	-0.182578

r/a	$\beta=-3$	$\beta=-2$	$\beta=-1$	$\beta=0$	$\beta=1$	$\beta=2$	$\beta=3$
1.2	0.	0.	0.	0.	0.	0.	0.
(Heat + Pressure) induced							
1.	-1.	-1.	-1.	-1.	-1.	-1.	-1.
1.04	-0.69157	-0.707689	-0.723436	-0.738762	-0.75362	-0.767968	-0.78177
1.08	-0.451881	-0.472466	-0.493105	-0.513715	-0.534215	-0.554524	-0.574564
1.12	-0.264346	-0.281996	-0.300135	-0.318704	-0.337637	-0.356868	-0.376324
1.16	-0.11675	-0.126905	-0.137591	-0.148794	-0.160496	-0.172674	-0.185303
1.2	0.	0.	0.	0.	0.	0.	0.
σ_θ/p_a							
Heat induced							
1.	-0.037651	-0.037898	-0.038158	-0.038430	-0.0387136	-0.0390076	-0.039311
1.04	-0.015797	-0.017592	-0.019488	-0.021484	-0.0235823	-0.025782	-0.028084
1.08	-0.001457	-0.002880	-0.004525	-0.006414	-0.0085684	-0.0110115	-0.013767
1.12	0.007832	0.0077524	0.0075095	0.0070664	0.0063806	0.0054037	0.004081
1.16	0.0137144	0.0153898	0.0172141	0.0191881	0.0213084	0.0235674	0.025952
1.2	0.0172962	0.0208196	0.0250539	0.0301413	0.0362513	0.0435871	0.052392
Pressure induced							
1.	3.40965	3.11182	2.82868	2.56044	2.30722	2.06903	1.84581
1.04	2.8453	2.70831	2.56918	2.4287	2.28763	2.14675	2.00681
1.08	2.4016	2.37983	2.35116	2.31576	2.27384	2.2257	2.17172
1.12	2.04936	2.11015	2.16665	2.21838	2.26487	2.30574	2.34066
1.16	1.76715	1.88698	2.00944	2.13397	2.25995	2.38675	2.51373
1.2	1.53909	1.70091	1.87463	2.06044	2.25843	2.46864	2.691
(Heat + Pressure) induced							
1.	3.372	3.07393	2.79052	2.52201	2.2685	2.03002	1.8065
1.04	2.82951	2.69072	2.5497	2.40721	2.26405	2.12097	1.97872
1.08	2.40015	2.37695	2.34664	2.30934	2.26527	2.21469	2.15795
1.12	2.05719	2.1179	2.17416	2.22544	2.27125	2.31115	2.34474
1.16	1.78086	1.90237	2.02666	2.15316	2.28126	2.41032	2.53968
1.2	1.55639	1.72173	1.89969	2.09058	2.29468	2.51222	2.74339
σ_{eq}/p_a							
(Heat + Pressure) induced							
1.	6.18294	5.7614	5.36061	4.98087	4.62236	4.2851	3.96899
1.04	4.97955	4.80607	4.62891	4.44908	4.26763	4.08557	3.90393
1.08	4.03338	4.02968	4.016	3.99241	3.95907	3.91626	3.86436
1.12	3.28315	3.39397	3.49919	3.59797	3.68953	3.77314	3.84816
1.16	2.68363	2.86983	3.06071	3.25545	3.45316	3.65291	3.8537
1.2	2.20107	2.4349	2.68657	2.95653	3.24517	3.55282	3.87974

Table 3 Comparison of the present results with the open literature [39] under combined loads

r (mm)	$1000u_r/a$			σ_r/p_a			σ_θ/p_a		
	[39]	[39] FEM	pres.	[39]	[39] FEM	pres.	[39]	[39] FEM	pres.
$\beta=-1$									
40.0	0.6698	0.6698	0.6698	-1.	-1.	-1.	0.67776	0.67972	0.67776
43.5	0.6497	0.6497	0.6497	-0.733	-0.733	-0.733	0.76688	0.76672	0.76688
47.5	0.6231	0.6231	0.6231	-0.487	-0.487	-0.487	0.81198	0.81187	0.81198
51.5	0.5949	0.5949	0.5949	-0.292	-0.292	-0.292	0.82416	0.82410	0.82416
55.5	0.5665	0.5665	0.5665	-0.137	-0.137	-0.137	0.81890	0.81885	0.81890
60.0	0.5355	0.5355	0.5355	0.	0.	0.	0.80236	0.80867	0.80236
$\beta=1$									
40.0	0.5187	0.5188	0.5187	-1.	-1.	-1.	0.13830	0.1367	0.13829
43.5	0.5121	0.5122	0.5120	-0.808	-0.808	-0.809	0.34923	0.34901	0.34923
47.5	0.5029	0.5031	0.5029	-0.601	-0.601	-0.601	0.59547	0.59540	0.59547
51.5	0.4917	0.4919	0.4917	-0.403	-0.403	-0.403	0.84718	0.84724	0.84718
55.5	0.4782	0.4784	0.4782	-0.212	-0.212	-0.212	1.10446	1.10464	1.10446
60.0	0.4597	0.4599	0.4597	0.	0.	0.	1.40083	1.39179	1.40083

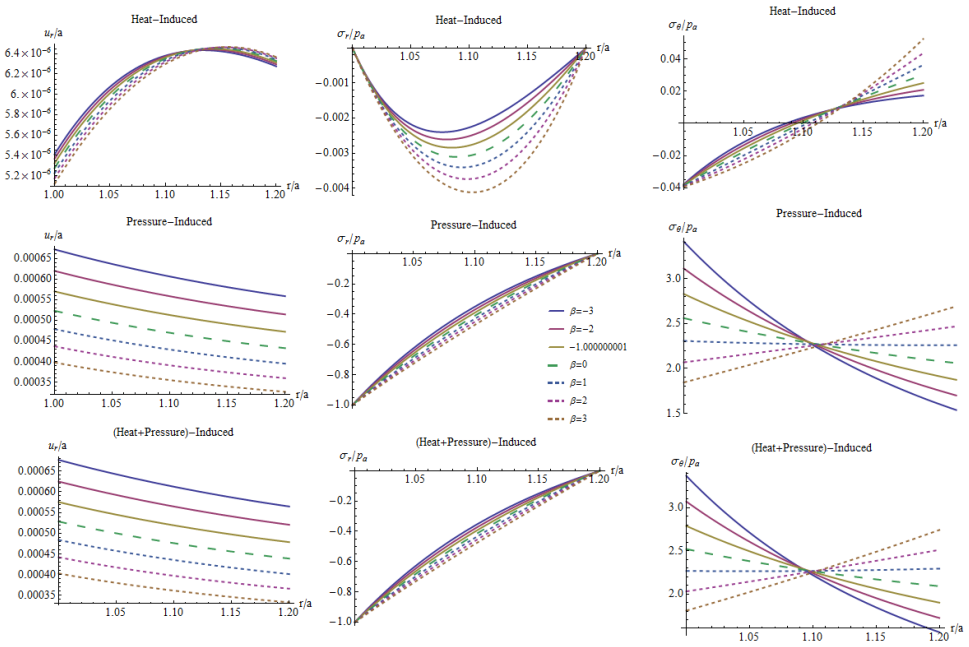

Figure 2 Elastic fields under separate and combined internal pressure and thermal loads for the first example [33]

As a second test example, Bayat et al. [39] problem is reconsidered. Their material and geometric data are: $a = 40\,\text{mm}$; $b = 60\,\text{mm}$, $\nu = 0.3$, $E_a = 200\,\text{GPa}$, $\alpha_a = 1.2 \cdot 10^{-6}\ 1/^\circ\,\text{C}$, $p_a = 80\ \text{MPa}$; $p_b = 0$, $T_a = 300^\circ\,\text{C}$; $T_b = 275^\circ\,\text{C}$; $\beta = -2,\ -1,\ 0,\ 1,\ 2$.

Bayat et al. also studied separate and combined effects of pressure and thermal loads. Table 3 shows the comparison of the present and Bayat et al.'s analytical and FEM results. A perfect accordance among the results are observed. The present results are illustrated in Fig. 3 with the addition of the graph of the equivalent stress. From Fig. 3, $\beta = 1$ seems to be an appropriate choice for the inhomogeneity index since it offers almost uniform radial distribution. In the second test example, since the temperature difference between the surfaces is much higher than the first example and the current sphere is thicker than the previous, thermal effects become much clearer. Because of this reason, the equivalent stresses are to be much higher than the combined hoop stresses which variations for both pressure and combined loads are very similar in Fig. 2, they are fairly different in Fig. 3.

6. Thermo-Mechanical Behavioral Differences Between a Sphere and a Cylinder

As stated above both References [33, 40] were used the same data in the first test example to study both cylinders [40] and spheres [33]. From those references the main differences in the behavior of cylinders and spheres may be observed. Eslami et al. [33] presented the equivalent stress variation for spheres which is in a good

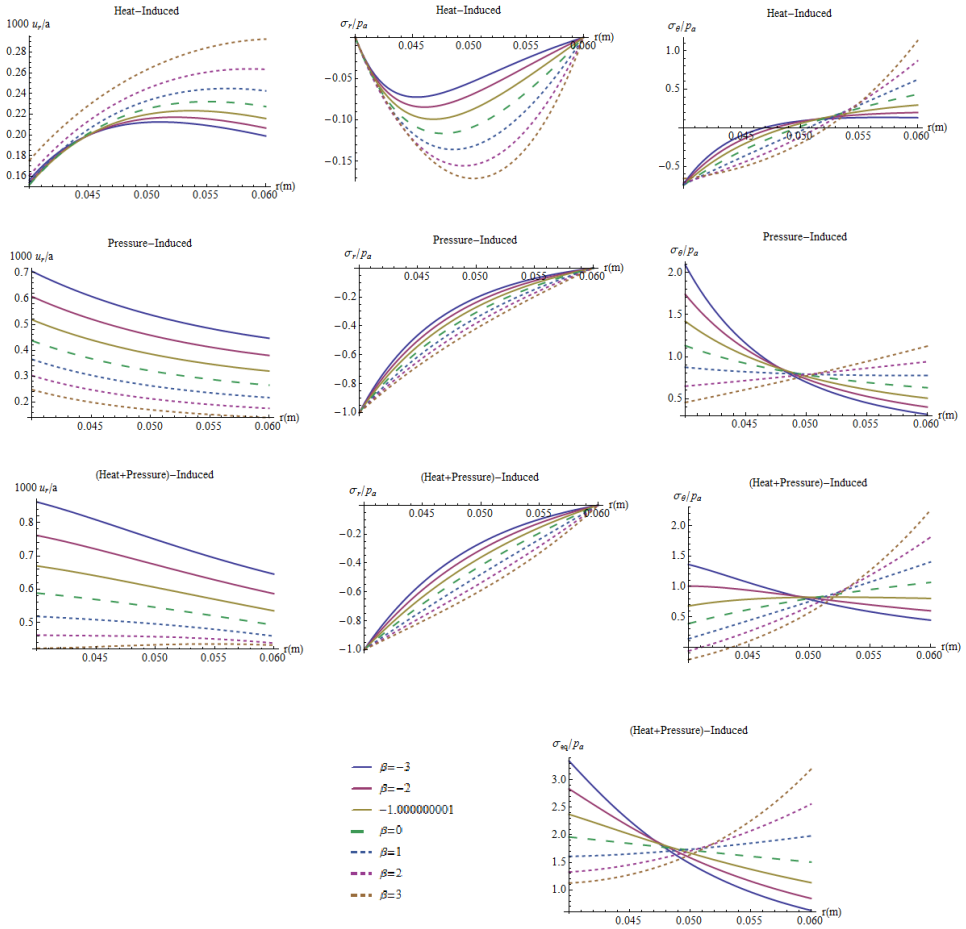

Figure 3 Elastic fields under separate and combined internal pressure and thermal loads for the second test example [39]

harmony with the present results as shown in Fig. 4. Table 4 comprises some numerical data to serve the aim of this section. As observed from both Fig. 4 and Tab. 4 that the elastic fields belonging a sphere, especially radial displacements and hoop stresses, are considerable less than cylinders. The maximum equivalent stress in a cylinder may be more than twice of a sphere. It may be noted that the present analytical results for spheres also overlaps the numerical results obtained by complementary functions method in the literature [42].

7. Thickness Effects

Eslami et al. [32] also presented three graphs for the equivalent stress variation for $b/a = 1.2$, 2 and 3 for the first test example. Those graphs showed that as the thickness increases the maximum equivalent stress decreases. In this section the second test example in [39] is reconsidered to study the thickness effects. Figures 5–7

Table 4 Comparison of the elastic fields of cylinders and spheres for combined pressure and thermal loads

	u_r/a		σ_r/p_a		σ_θ/p_a	
r/a	$\beta = -2$	$\beta = 2$	$\beta = -2$	$\beta = 2$	$\beta = -2$	$\beta = 2$
	Cylinder – after [Jabbari et al. / analytical [40] and Çelebi et al. / numerical [41]]					
1.	0.00161944	0.00114082	-1	-1	6.62127	4.51743
1.04	0.00158667	0.00111628	-0.722291	-0.784165	5.84288	4.70652
1.08	0.00155679	0.00109454	-0.491571	-0.577254	5.19022	4.89893
1.12	0.00152961	0.00107516	-0.29876	-0.378189	4.63928	5.09474
1.16	0.00150494	0.00105779	-0.136767	-0.186042	4.1713	5.29405
1.2	0.00148263	0.00104213	0	0	3.77145	5.49697
	Sphere [present/analytical]					
1.	0.000624937	0.00044225	-1	-1	3.07393	2.03002
1.04	0.000598606	0.00042222	-0.707689	-0.767968	2.69072	2.12097
1.08	0.000575302	0.00040509	-0.472466	-0.554524	2.37695	2.21469
1.12	0.000554712	0.00039034	-0.281996	-0.356868	2.1179	2.31115
1.16	0.000536571	0.00037755	-0.126905	-0.172674	1.90237	2.41032
1.2	0.000520652	0.00036637	0	0	1.72173	2.51222

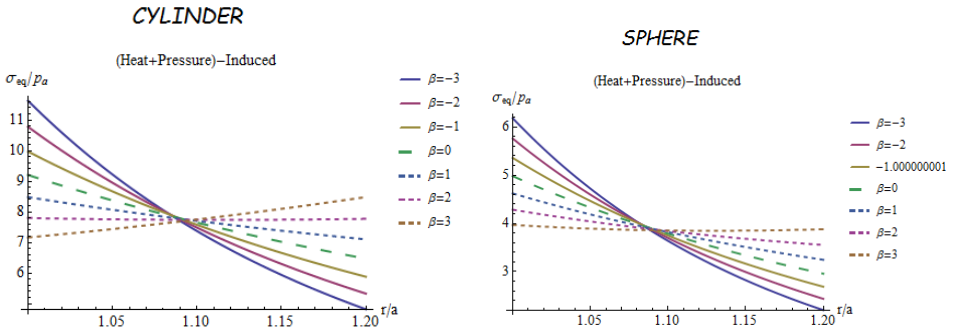

Figure 4 Comparison of the equivalent stress variation for both cylinders and spheres under combined effects of pressure and thermal loads

illustrate the variation of the radial displacement, radial stress, and hoop stress with the thickness under separate and combined loads, respectively. Thickness effect on the equivalent stress under combined loads is shown in Fig. 8.

From Fig. 5, it is observed that as the wall thickness decreases, radial displacement increases under pressure loads. The maximum radial displacement due to the internal pressure is always at the inner surface. The converse is true for only thermal loads. A decrease in the wall thickness results in a decrease in the radial thermal displacements. The location of the maximum radial thermal displacement may shift towards the intermediate surfaces if absolutely higher negative inhomogeneity indexes are considered. For thin-walled spheres and all inhomogeneity indexes, the maximum radial thermal displacement is always at the outer surface. When the thickness increases, the radial displacement variation becomes different regarding to the sign of inhomogeneity indexes under combined loads. For instance, for $a/b = 0.5$ and negative inhomogeneity indexes, the maximum combined radial stress is at the inner surface while it is at the outer surface for positive inhomogeneity indexes.

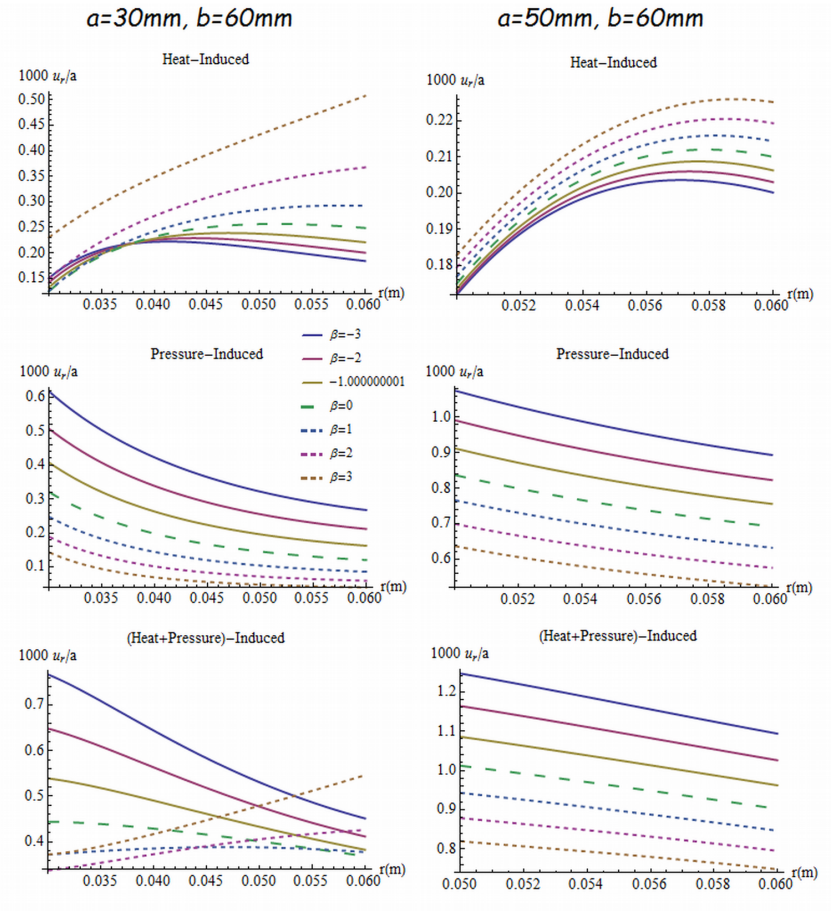

Figure 5 Variation of the radial displacements with the thickness under separate and combined loads

From Fig. 6 it is observed that when the thickness increases, the variation of radial stress with respect to the inhomogeneity indexes may be more noticeable. As expected, the maximum radial stress due to the inner pressure is at the inner surface while the radial thermal stress is at the vicinity of the middle surface. As the thickness decreases, the values of the radial thermal stresses also decrease. However, the values of the radial stress due to the combined loads become much higher at the intermediate surfaces than the thicker spheres. The radial stresses are all in compression under both separate and combined loads.

From Fig. 7 it is observed that as the thickness decreases, the values of the hoop stresses increase under separate thermal and pressure loads. While the radial thermal stresses are all in compression (Fig. 6), the thermal hoop stresses may be compression-tension in character. Pressure loads present the hoop stresses in tension. The hoop stress in a thin-walled sphere under combined loads is also in tension. However, thick spheres and positive inhomogeneity indexes may offer

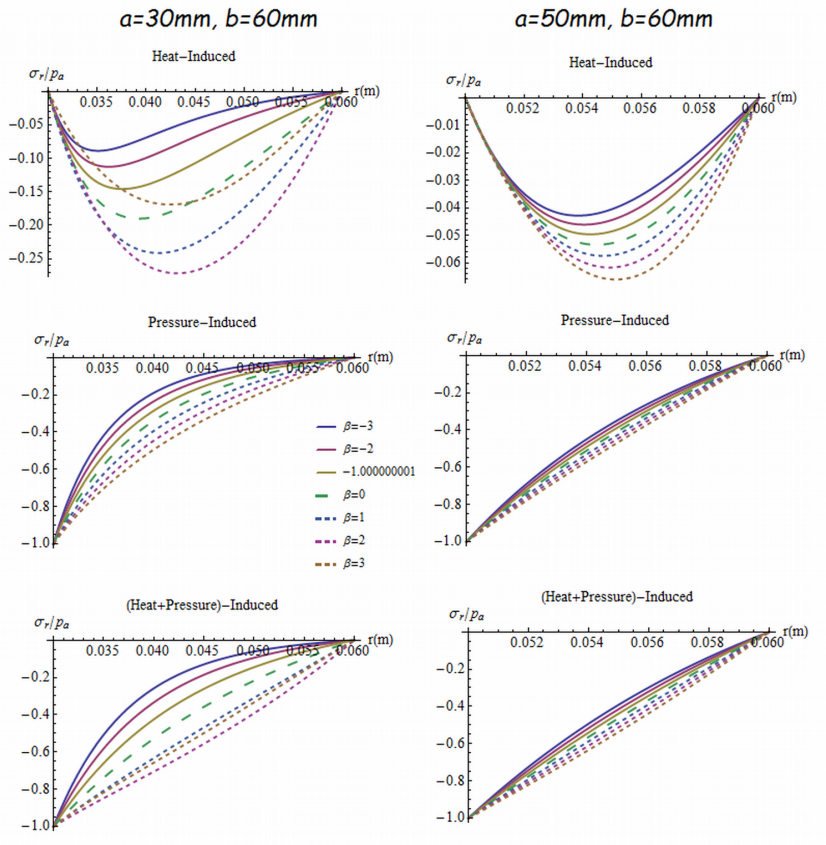

Figure 6 Variation of the radial stress with the thickness under separate and combined loads

combined hoop stresses in both compression and tension. Combined loads give the higher hoop stresses when the thickness decreases.

Figure 8 suggests that as the thickness decreases the equivalent stress increases. For this example $\beta = 1$ may be assumed as a better choice for both thin-walled and thick-walled spheres.

8. Examples with Physical Materials

In this section three types of physical metal and ceramics are studied for the thermomechanical analysis of spheres, Tab. 5. It is assumed that the inner surface is full ceramic and the outer is full metal. The properties of the grading of metal and ceramic at the intermediate surfaces obey the simple-power law in Eq. (8). Hypothetically chosen inhomogeneity indexes are no longer used in this section. The inhomogeneity indexes now should be determined from the following equation

$$\beta = \frac{\ln \frac{E_a}{E_b}}{\ln \frac{a}{b}}; \quad n = \frac{\ln \frac{\alpha_a}{\alpha_b}}{\ln \frac{a}{b}}; \quad \mu = \frac{\ln \frac{k_a}{k_b}}{\ln \frac{a}{b}}. \tag{28}$$

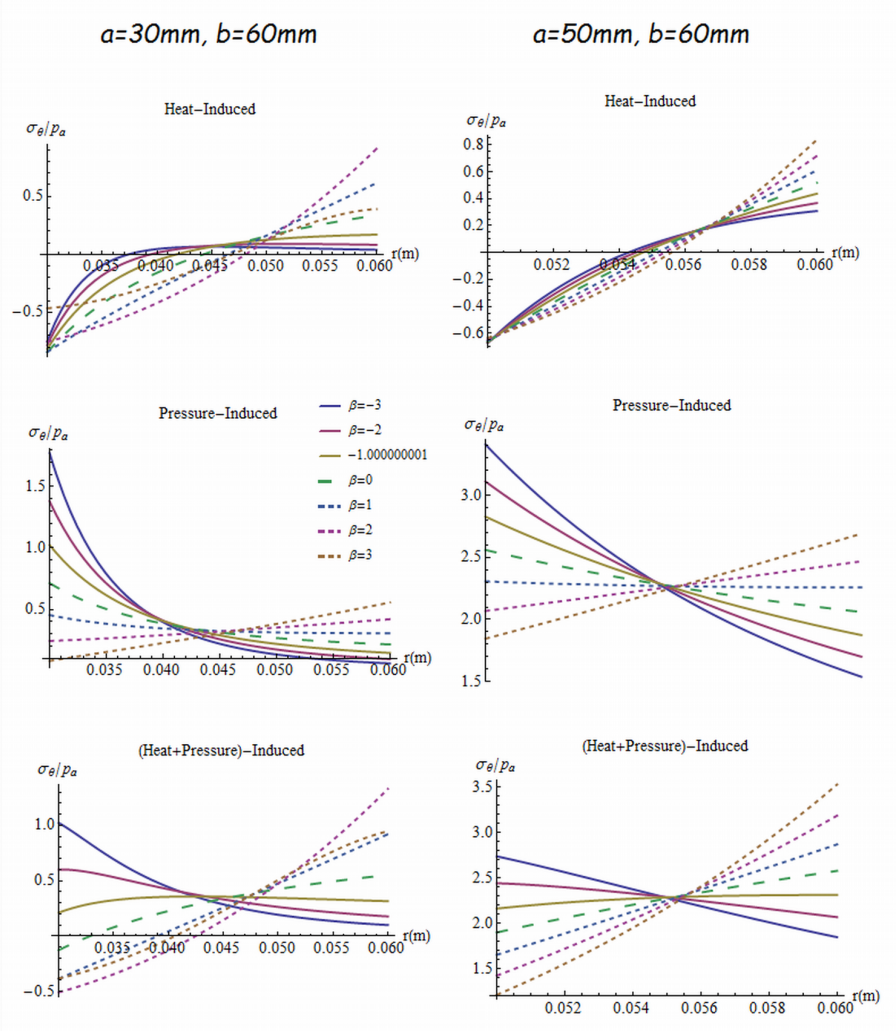

Figure 7 Variation of the hoop stress with the thickness under separate and combined loads

As seen from Eq. (28) the values of the inhomogeneity indexes may change with the aspect ratio of the sphere for even the same FGM. As the thickness decreases, values of the inhomogeneity indexes increase for the same material. Location of constituents defines the sign of the inhomogeneity indexes (Tab. 6). For instance if the inner surface is full ceramic and the outer is full metal, β becomes negative. This means that Young's modulus decreases from the inner surface towards the outer. The converse is true if the inner surface is full metal and the outer is full ceramic. In these section geometrical properties of the sphere, internal and external pressures, and prescribed temperatures at its both surfaces are assumed to be: $p_a = 30\,\mathrm{MPa}$; $p_b = 5\,\mathrm{MPa}$; $T_a = 373\,\mathrm{K}$; $T_b = 273\,\mathrm{K}$; $a = 0.5$; $b = 1.0\,\mathrm{m}$. The results are presented in Figs. 9–10 and Tab. 7.

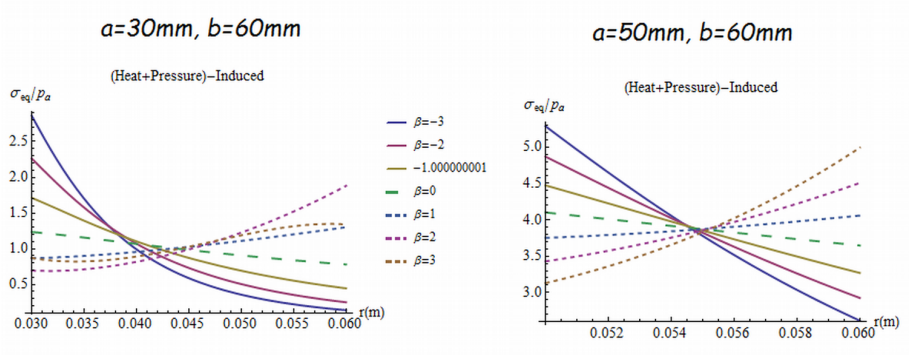

Figure 8 Variation of the equivalent stress with the thickness under combined loads

Table 5 The physical constituent material properties

		E	ρ	ν	k	α
		GPa	kg/m^3	[-]	W/mK	1/K·10^{-6}
	Nickel *(Ni)*	199.5	8900	0.3	90.7	13.3
Metals	Aluminum *(Al)*	70	2700	0.3	204	23.
	Stainless Steel *(SUS304)*	201.04	7800	0.3262	15.379	12.33
	Silicon Nitride *(Si_3N_4)*	348.43	4429	0.24	1.209	5.8723
Ceramics	Aluminum Oxide *(Al_2O_3)*	393	3970	0.3	30.1	8.8
	Zirconium oxide *(ZrO_2)*	116.4	3657	0.3	1.78	8.7

Table 6 Inhomogeneity indexes for physical metal-ceramic pairs, $a = 0.5\,\text{m}$, $b = 1\,\text{m}$

The inner surface is full ceramic; the outer is full metal			
	β	n	μ
Ni/Si_3N_4 (FGM-1)	−0.80448	1.17943	6.22922
Al/Al_2O_3 (FGM-2)	−2.48910	1.38606	2.76073
$SUS304/ZrO_2$ (FGM-3)	0.78839	0.50309	3.11101

Variation of the radial displacements under separate and combined loads for physical FGMs is seen in Fig. 9. Ni/Si_3N_4 offers the smallest radial displacements under separate and combined loads.

As seen from Fig. 10, while metal and ceramic offers individually radial thermal stresses in compression, the FGM offers the radial thermal stress in tension. $SUS304 - ZrO_2$ gives better radial thermal and combined stresses than the other FGMs. Generally, both radial thermal stresses and thermal hoop stresses are found much higher than the radial stresses due to the pressures. If combined effects of the loads are considered, the radial and hoop stresses in FGMs may be in tension-compression. $SUS304 - ZrO_2$ again present better solutions for separate and combined thermal hoop stresses for FGM spheres.

Table 7 Elastic fields for physical FGMs

Thermal				Pressure			Thermal+Pressure		
r/b	Si_3N_4	FGM-1	Ni	Si_3N_4	FGM-1	Ni	Si_3N_4	FGM-1	Ni
u_r (mm)									
0.5	0.8855	1.3795	2.00545	0.0244	0.029951	0.0451	0.9098	1.4095	2.0506
0.6	1.1051	1.5655	2.51632	0.0164	0.020951	0.0306	1.1215	1.5865	2.5469
0.7	1.2916	1.8010	2.94157	0.0115	0.015012	0.0217	1.3031	1.816	2.9633
0.8	1.4604	2.0949	3.32119	0.0082	0.010763	0.0159	1.4686	2.1057	3.3371
0.9	1.6188	2.4432	3.67428	0.0059	0.007522	0.0118	1.6248	2.4508	3.6861
1.	1.7709	2.8412	4.0109	0.0042	0.004916	0.0088	1.7751	2.8461	4.0197
σ_r (GPa)									
0.5	0.	0.	0.	-0.03	-0.03	-0.03	-0.03	-0.03	-0.03
0.6	-0.040	0.0770	-0.05616	-0.018	-0.0172	-0.018	-0.058	0.0598	-0.074
0.7	-0.042	0.0936	-0.05873	-0.012	-0.01114	-0.012	-0.054	0.0825	-0.071
0.8	-0.031	0.0757	-0.04315	-0.008	-0.00796	-0.008	-0.039	0.0678	-0.052
0.9	-0.016	0.0414	-0.02199	-0.006	-0.00613	-0.006	-0.022	0.0353	-0.028
1.	0.	0.	0.	-0.005	-0.005	-0.005	-0.005	-0.005	-0.005
σ_θ (GPa)									
0.5	-0.192	0.2714	-0.27075	0.0129	0.017495	0.0129	-0.179	0.2889	-0.258
0.6	-0.083	0.2058	-0.11632	0.0068	0.008041	0.0068	-0.076	0.2138	-0.109
0.7	-0.018	0.0774	-0.02479	0.0038	0.003687	0.0038	-0.014	0.0811	-0.021
0.8	0.0249	-0.037	0.035113	0.0021	0.001455	0.0021	0.0270	-0.036	0.0372
0.9	0.0548	-0.134	0.077177	0.0010	0.000219	0.0010	0.0558	-0.133	0.0782
1.	0.0769	-0.216	0.1083	0.0004	-0.0005	0.0004	0.0773	-0.216	0.1087
r/b	Al_2O_3	FGM-2	Al	Al_2O_3	FGM-2	Al	Al_2O_3	FGM-2	Al
u_r (mm)									
0.5	1.3269	2.1200	3.46807	0.0229	0.038187	0.1286	1.3498	2.1582	3.5966
0.6	1.6649	2.4213	4.35153	0.0155	0.028008	0.0872	1.6805	2.4493	4.4388
0.7	1.9463	2.8338	5.08693	0.0110	0.020453	0.0620	1.9573	2.8543	5.1489
0.8	2.1975	3.3539	5.74342	0.0081	0.014197	0.0453	2.2056	3.3681	5.7887
0.9	2.4311	3.9759	6.35402	0.0060	0.008521	0.0336	2.4371	3.9844	6.3876
1.	2.6538	4.6937	6.93614	0.0045	0.002990	0.025	2.6583	4.6967	6.9611
σ_r (GPa)									
0.5	0.	0	0.	-0.03	-0.03	-0.03	-0.03	-0.03	-0.03
0.6	-0.073	0.1038	-0.0341	-0.018	-0.0153	-0.018	-0.091	0.0884	-0.052
0.7	-0.077	0.1014	-0.0356	-0.012	-0.0097	-0.012	-0.088	0.0917	-0.047
0.8	-0.056	0.0701	-0.0262	-0.008	-0.00715	-0.008	-0.065	0.0629	-0.035
0.9	-0.029	0.0338	-0.0133	-0.006	-0.00580	-0.006	-0.035	0.0280	-0.020
1.	0.	0	0.	-0.005	-0.005	-0.005	-0.005	-0.005	-0.005
σ_θ (GPa)									
0.5	-0.353	0.5376	-0.1643	0.0129	0.030021	0.0129	-0.340	0.5677	-0.151
0.6	-0.152	0.1930	-0.07058	0.0068	0.010070	0.0068	-0.145	0.2031	-0.064
0.7	-0.032	0.0199	-0.01504	0.0038	0.002933	0.0038	-0.029	0.0228	-0.011
0.8	0.0458	-0.073	0.021306	0.0021	0.000028	0.0021	0.0478	-0.073	0.0234
0.9	0.1006	-0.127	0.046829	0.0010	-0.00125	0.0010	0.1016	-0.128	0.0479
1.	0.1412	-0.159	0.065714	0.0004	-0.00184	0.0004	0.1415	-0.160	0.0661

9. Conclusions

For a power-law-graded thick-walled sphere under separate and combined internal/external pressure and steady-state thermal loads due to the surface temperature differences, an analytical thermo-mechanical study accompanying a comprehensive parametric studies with hypothetical and physical inhomogeneity indexes is performed in the present work.

The studies with hypothetic inhomogeneity indexes revealed that finding a proper choice for the inhomogeneity indexes seems to be possible according to the values of thermal and pressure loads including aspect ratios of the sphere. For instance, while $\beta = 3$ is assumed as a better inhomogeneity index in the first test example, $\beta = 1$ is found as the best for the second test example. Besides thermal effects may become more influential when the surface temperature differences are

Table 8 Continued from Table 7

	Thermal			Pressure			Thermal+Pressure		
r/b	ZrO_2	FGM-3	SUS304	ZrO_2	FGM-3	SUS304	ZrO_2	FGM-3	SUS304
u_r (mm)									
0.5	1.3118	1.5920	1.85919	0.0773	0.065118	0.0459	1.3892	1.6571	1.9051
0.6	1.6460	1.8966	2.33888	0.0525	0.042640	0.0312	1.6985	1.9392	2.3701
0.7	1.9242	2.1901	2.73446	0.0373	0.029850	0.0223	1.9615	2.220	2.7568
0.8	2.1725	2.4968	3.08521	0.0272	0.021951	0.0164	2.1997	2.5187	3.1016
0.9	2.4035	2.8223	3.40988	0.0202	0.016768	0.0123	2.4237	2.8391	3.4222
1.	2.6237	3.1674	3.71838	0.0150	0.013204	0.0093	2.6387	3.1806	3.7277
σ_r (GPa)									
0.5	0.	0.	0.	-0.03	-0.03	-0.03	-0.03	-0.03	-0.03
0.6	-0.021	0.0045	-0.0545	-0.018	-0.01880	-0.018	-0.039	-0.014	-0.072
0.7	-0.022	0.0115	-0.0570	-0.012	-0.01265	-0.012	-0.034	-0.001	-0.069
0.8	-0.016	0.0134	-0.0419	-0.008	-0.00895	-0.008	-0.025	0.0044	-0.050
0.9	-0.008	0.0093	-0.0213	-0.006	-0.00659	-0.006	-0.015	0.0027	-0.028
1.	0.	0.	0.	-0.005	-0.005	-0.005	-0.005	-0.005	-0.005
σ_θ (GPa)									
0.5	-0.103	-0.010	-0.26278	0.0129	0.008395	0.0129	-0.090	-0.002	-0.250
0.6	-0.044	0.0291	-0.11290	0.0068	0.005335	0.0068	-0.038	0.0344	-0.106
0.7	-0.009	0.0284	-0.02406	0.0038	0.003657	0.0038	-0.006	0.0320	-0.020
0.8	0.013	0.0087	0.034079	0.0021	0.002654	0.0021	0.0155	0.0113	0.0361
0.9	0.0295	-0.021	0.074904	0.0010	0.002014	0.0010	0.0305	-0.019	0.0759
1.	0.0413	-0.058	0.105111	0.0004	0.001585	0.0004	0.0417	-0.057	0.1055

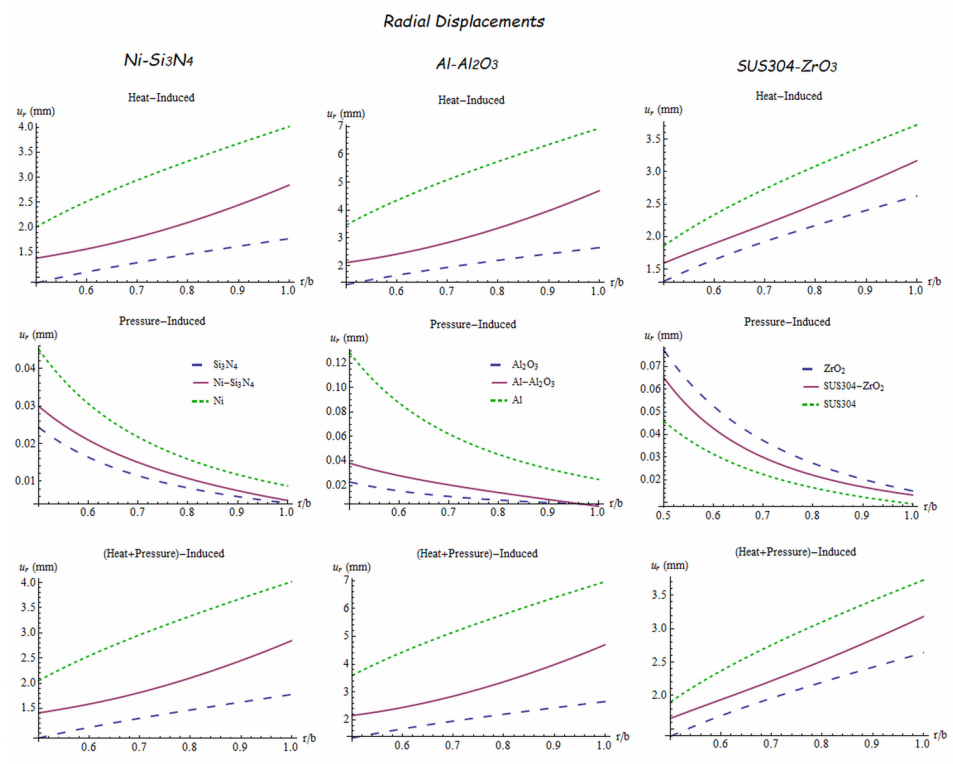

Figure 9 Variation of the radial displacements under separate and combined loads for physical FGMs

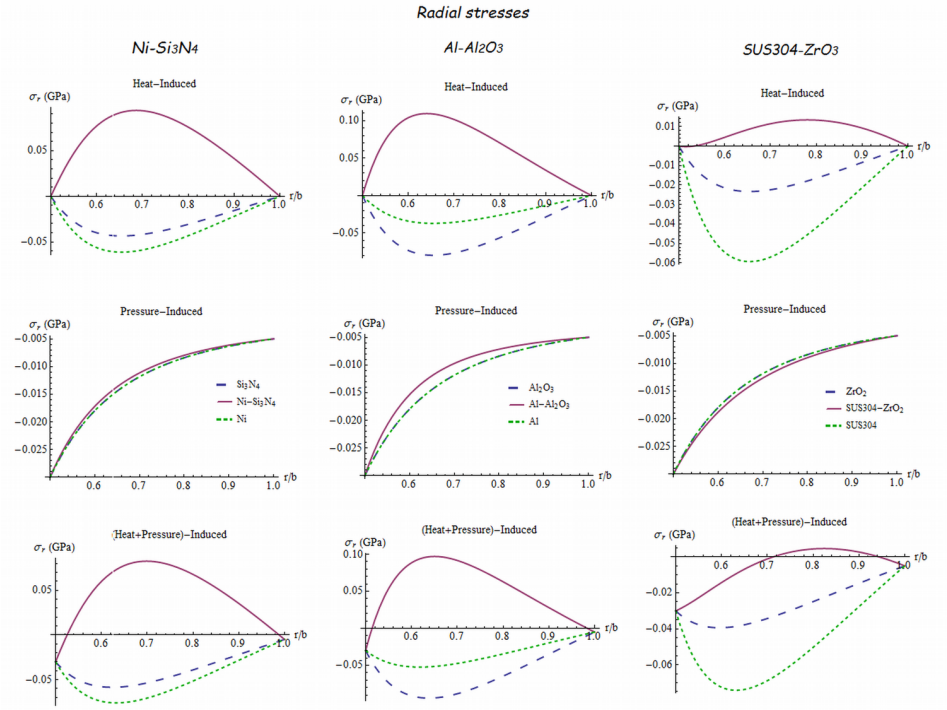

Figure 10 Variation of the radial and hoop stress under separate and combined loads for physical FGMs

higher and the sphere is thicker.

Spheres offer much smaller elastic fields than cylinders under the same conditions. The maximum equivalent stress in a cylinder may be more than twice of a sphere. Thickness effects seem to be play a significant role in the variation of the elastic fields along he radial coordinate.

As the wall thickness decreases, the radial displacements increase under pressure loads and decrease under thermal loads. For thin-walled spheres and all inhomogeneity indexes, the maximum radial thermal displacement is always at the outer surface. The maximum radial displacement due to the internal pressure is always at the inner surface. The maximum radial stress due to the inner pressure is at the inner surface while the radial thermal stress is at the vicinity of the middle surface. The radial thermal stresses decrease with decreasing thicknesses. The radial stresses are all in compression under both separate and combined loads.

The hoop stresses increase with decreasing thicknesses under separate thermal and pressure loads. While the radial thermal stresses are all in compression, the thermal hoop stresses may be compression-tension in character. Pressure loads present the hoop stresses in tension.

As the thickness decreases the equivalent stress increases. For the second example $\beta = 1$ may be assumed as a better choice for both thin-walled and thick-walled spheres.

It is also disclosed that while either metal or ceramic individually offers radial thermal stresses in compression, the FGM offers the radial thermal stress in tension. For the example considered, $SUS304 - ZrO_2$ presents better solutions for separate and combined hoop and radial stresses than Ni/Si_3N_4 and Al/Al_2O_3 in FGM spheres.

References

[1] **Timoshenko, S.P., Goodier, J.N.**: *Theory of Elasticity*, 3rd Edition, New York: McGraw-Hill, **1970**.

[2] **Borisov, A.V.**: Elastic analysis of multilayered thick-walled spheres under external load, *Mechanika*, **4**(84), 28–32, **2010**.

[3] **Gamer, U.**: The expansion of the elastic-plastic spherical shell with nonlinear hardening, *Int J Mech Sci*, **30**(6), 415–426, **1988**.

[4] **Megahed, M.M.**: Elastic-plastic behaviour of spherical shells with nonlinear hardening properties, *Int J Solids Struct*, **27**(12), 1499–1514, **1991**.

[5] **Gao, X.L.**: Strain gradient plasticity solution for an internally pressurized thick walled spherical shell of an elastic-plastic material, *Mech. Res. Commun.*, **30**, 411–420, **2003**.

[6] **Yildirim, V.**: Heat-induced, pressure-induced and centrifugal-force-induced exact axisymmetric thermo-mechanical analyses in a thick-walled spherical vessel, an infinite cylindrical vessel, and a uniform disk made of an isotropic and homogeneous material, *International Journal of Engineering & Applied Sciences (IJEAS)*, **9**(2), 66–87, **2017**.

[7] **Chen, W.Q.**: Stress distribution in a rotating elastic functionally graded material hollow sphere with spherical isotropy, *The Journal of Strain Analysis*, **35**(1), 13–20, **2000**.

[8] **Guven, U., Baykara, C.**: On stress distributions in functionally graded isotropic spheres subjected to internal pressure, *Mech Res Commun*, **28**(3), **2001**, 277–281.

[9] **You, L.H., Zhang J.J., You X.Y.**: Elastic analysis of internally pressurized thick-walled spherical pressure vessels of functionally graded materials, *Int. J. Pressure Vessel Piping*, **82**(5), 347–354, **2005**.

[10] **Chen, Y.Z., Lin, X.Y.**: Elastic analysis for thick cylinders and spherical pressure vessels made of functionally graded materials, *Comput. Mater. Sci.*, **44**(2), 581–587, **2008**.

[11] **Tutuncu N., Temel, B.**: A novel approach to stress analysis of pressurized FGM cylinders, disks and spheres, *Compos. Struct.*, **91**, 385–390, **2009**.

[12] **Li, X.F., Peng, X.L., Kang, Y.A.**: Pressurized hollow spherical vessels with arbitrary radial nonhomogeneity, *AIAA Journal*, **47**(9), 2262–2266, **2009**.

[13] **Saidi, A.R., Atashipour, S.R., Jomehzadeh, E.**: Exact elasticity solutions for thick-walled FG spherical pressure vessels with linearly and exponentially varying properties, *IJE Transactions A: Basics*, **22**(4), 405–416, **2009**.

[14] **Chen, Y.Z., Lin, X.Y.**: An alternative numerical solution of thick-walled cylinders and spheres made of functionally graded materials, *Comput. Mater. Sci,* **48**, 640–647, **2010**.

[15] **Nie, G.J., Zhong, Z., Batra, R.C.**: Material tailoring for functionally graded hollow cylinders and spheres, *Compos. Sci. Technol.*, **71**(5), 666–673, **2011**.

[16] **Nejad, M.Z., Abedi, M., Lotfian, M.H., Ghannad, M.**: An exact solution for stresses and displacements of pressurized FGM thick-walled spherical shells

with exponential-varying properties, *Journal of Mechanical Science and Technology*, **26**(12), 4081–4087, **2012**.

[17] **Ghannad, M., Nejad, M.Z.**: Complete closed-form solution for pressurized heterogeneous thick spherical shells, *Mechanika*, **18**(5), 508–516, **2012**.

[18] **Karami, K., Abedi, M., Nejad, M.Z., Lotfian, M.H.**: Elastic analysis of heterogeneous thick-walled spherical pressure vessels with parabolic varying properties, *Front. Mech. Eng.*, **7**(4), 433–438, **2012**.

[19] **Nejad, M.Z., Rastgoo, A., Hadi, A.**: Effect of exponentially-varying properties on displacements and stresses in pressurized functionally graded thick spherical shells with using iterative technique, *Journal of Solid Mechanics*, **6**(4), 366–377, **2014**.

[20] **Anani, Y., Rahimi, G.H.**: Stress analysis of thick pressure vessel composed of functionally graded incompressible hyperelastic materials, *Int. J. Mech. Sci.*, **104**, 1–7, **2015**.

[21] **Shrivastava, S.K., Sondhi, L., Tiwari, J.K.**: Elastic analysis of rotating spherical pressure vessel of functionally graded material modeled by Mori-Tanaka scheme, *International J. of Eng. Research & Indu. Appls. (IJERIA)*, **9**(III), 1–12, **2016**.

[22] **Norouzi, M., Amiri Delouei, A., Seilsepour, M.**: A general exact solution for heat conduction in multilayer spherical composite laminates, *Compos. Struct.*, **106**, 288–295, **2013**.

[23] **Singh, S., Jain, P.K., Rizwan-Uddin**: Analytical solution to transient heat conduction in polar coordinates with multiple layers in radial direction, *Int. J. Therm. Sci.*, **47**, 261–273, **2008**.

[24] **Jain, P.K., Singh, S., Rizwan-uddin.**: An exact analytical solution for two dimensional, unsteady, multilayer heat conduction in spherical coordinates, *Int. J. Heat Mass Transfer*, **53**, 2133–2142, **2010**.

[25] **Lu, X., Viljanen, M.**: An analytical method to solve heat conduction in layered spheres with time-dependent boundary conditions, *Physics Letters A*, **351**, 274–282, **2006**.

[26] **Yildirim V.**: Exact thermal analysis of functionally graded cylindrical and spherical vessels, *International Journal of Engineering & Applied Sciences (IJEAS)*, **9**(2), 112–126, **2017**.

[27] **Cheung, J.B., Chen, T.S., Thirumalai, K.**: Transient thermal stresses in a sphere by local heating, *J. Appl. Mech.*, **41**(4), 930–934, **1974**.

[28] **Takeuti, Y., Tanigawa, Y.**: Transient thermal stresses of a hollow sphere due to rotating heat source, *J. Therm. Stress.*, **5**(3-4), 283–298, **1982**.

[29] **Obata, Y., Noda, N.**: Steady thermal stress in a hollow circular cylinder and a hollow sphere of a functionally gradient materials, *J. Therm. Stress.*, **17**(3), 3471–3487, **1994**.

[30] **Lutz, M.P., Zimmerman, R.W.**: Thermal stresses and effective thermal expansion coefficient of a functionally graded sphere, *J. Therm. Stress.*, **19**(1), 39–54, **1996**.

[31] **Tsai, C.S., Lin, Y.C., Hung, C.I.**: A study on the non-Fourier effects in spherical media due to sudden temperature changes on the surfaces. *Heat Mass Transfer*, **41**, **2005**, 709–716.

[32] **Bagri, A., Eslami, M.R.:** A unified generalized thermoelasticity; solution for cylinders and spheres, *Int. J. Mech. Sci.*, **49**, 1325–1335, **2007**.

[33] **Eslami, M.R., Babaei, M.H., Poultangari, R.**: Thermal and mechanical stresses in a functionally graded thick sphere, *Int. J. Pressure Vessel Piping*, **82**, 522–527, **2005**.

[34] **Poultangari, R., Jabbari, M., Eslami, M.R.**: Functionally graded hollow spheres under non-axisymmetric thermomechanical loads, *Int. J. Pressure Vessel Piping*, **85**(5), 295–305, **2008**.

[35] **Alavi, F., Karimi, D., Bagri, A.**: An investigation on thermoelastic behaviour of functionally graded thick spherical vessels under combined thermal and mechanical loads, *Journal of Achievements in Materials and Manufacturing Engineering*, **31**(2), 422–428, **2008**.

[36] **Jabbari, M., Dehbani, H., Eslami, M.R.**: An exact solution for classic coupled thermoelasticity in spherical coordinates, *Journal of Pressure Vessel Technology*, **132**, 031201-11, **2010**.

[37] **Nayak, P., Mondal, S.C., Nandi, A.**: Stress, strain and displacement of a functionally graded thick spherical vessel, *International Journal of Engineering Science and Technology (IJEST)*, **3**(4), 2659–2671, **2011**.

[38] **Jabbari, M., Karampour, S., Eslami, M.R.**: Radially symmetric steady state thermal and mechanical stresses of a poro FGM hollow sphere, *International Scholarly Research Network, ISRN Mechanical Engineering*, Article ID 305402 (7 pages), **2011**.

[39] **Bayat, Y., Ghannad, M., Torabi, H.**: Analytical and numerical analysis for the FGM thick sphere under combined pressure and temperature loading, *Arch. Appl. Mech.*, **82**, 229–242, **2012**.

[40] **Jabbari, M., Sohrabpour, S., Eslami, M.R.**: Mechanical and thermal stresses in a functionally graded hollow cylinder due to radially symmetric loads, *Int. J. Pressure Vessel Piping*, **79**(7), 493–497, **2002**.

[41] **Celebi, K., Yarimpabuc, D., Keles, I.**: A novel approach to thermal and mechanical stresses in a FGM cylinder with exponentially-varying properties, *Journal of Theoretical and Applied Mechanics*, **55**(1), 343–351, **2017**.

[42] **Celebi, K., Yarimpabuc, D., Keles, I.**: A unified method for stresses in FGM sphere with exponentially-varying properties, *Structural Engineering and Mechanics*, **57**(5), 823–835, **2016**.

Appendix A

Solution of

$$\frac{2}{r}T'(r) + T''(r) = 0$$

under boundary conditions, $T(a) = T_a$ and $T(b) = T_b$, gives the following for a sphere made of a homogeneous and isotropic material [6].

$$T(r) = -\frac{1}{r}\frac{ab(T_a - T_b)}{(a-b)} + \frac{aT_a - bT_b}{a-b} \qquad \text{(A.1)}$$

Appendix B

For a sphere made of an isotropic and homogeneous material, solution of the following under boundary conditions, $\sigma_r(a) = -p_a$ and $\sigma_r(b) = -p_b$,

$$u_r''(r) + \frac{2}{r}u_r'(r) - \frac{2}{r^2}u_r(r) = 0 \qquad \text{(A.2)}$$

offers the elastic field due to both internal and external pressures as follows [26]

$$u_r(r) = \frac{(2\nu^2+\nu-1)}{2r^2E(\lambda-1)(2\lambda+1)(\nu-1)(a^3-b^3)}\begin{pmatrix} a^3p_a\left(b^3(2\lambda+1)-2(\lambda-1)r^3\right) \\ -b^3p_b\left(a^3(2\lambda+1)-2(\lambda-1)r^3\right)\end{pmatrix}$$

$$\sigma_r(r) = \frac{1}{r^3(a^3-b^3)}\left(a^3p_a(b^3-r^3) + b^3p_b(a^3-r^3)\right) \qquad \text{(A.3)}$$

$$\sigma_\theta(r) = \frac{1}{2r^3(a^3-b^3)}\left(-a^3p_a(b^3+2r^3) + b^3p_b(a^3+2r^3)\right)$$

Finally, for a sphere made of an isotropic and homogeneous material, solution of the following under boundary conditions, $\sigma_r(a) = 0$ and $\sigma_r(b) = 0$,

$$u_r''(r) + \frac{2}{r}u_r'(r) - \frac{2}{r^2}u_r(r) = (1+2\lambda)\alpha T'(r) = \frac{1}{r^2}\frac{ab(T_a-T_b)\alpha(1+2\lambda)}{(a-b)} \qquad \text{(A.4)}$$

presents the steady-state elastic field of the sphere having surface temperatures, $T(a) = T_a$ and $T(b) = T_b$, as follows [26]

$$u_r(r) = \frac{\begin{pmatrix} a^3\left(\alpha(\nu+1)\left(b^3(2\lambda+1)(T_a-T_b) - 2(\lambda-1)r^3T_a\right) - 2(2\lambda+1)(\nu-1)\Omega\left((\lambda-1)r^2 - b^2\lambda\right)\right) \\ -2a^2\lambda(\nu-1)\Omega\left(b^3(2\lambda+1) - 2(\lambda-1)r^3\right) \\ +2b^2(\lambda-1)r^2\left((\nu-1)\Omega(2b\lambda+b-2\lambda r) + \alpha b(\nu+1)rT_b\right)\end{pmatrix}}{2(\lambda-1)(2\lambda+1)(\nu-1)r^2(a^3-b^3)}$$

$$\sigma_r(r) = \frac{E(a-r)(b-r)(a(b+r)+br)\left(2\lambda(\nu-1)\Omega(a-b) + ab\alpha(\nu+1)(T_a-T_b)\right)}{(2\nu^2+\nu-1)r^3(a^3-b^3)} \qquad \text{(A.5)}$$

$$\sigma_\theta(r) = \frac{E\begin{pmatrix} -2(\nu-1)\Omega(a-b)(a^2(b^2\lambda+(\lambda+1)r^2) + ar^2(b\lambda+b-2\lambda r) + br^2(b\lambda+b-2\lambda r) \\ -ab\alpha(\nu+1)(T_a-T_b)\left(2r^2(a^2+ab+b^2) + a^2b^2 - 2r^3(a+b)\right)\end{pmatrix}}{2(2\nu^2+\nu-1)r^3(a^3-b^3)}$$

where $\Omega = \frac{ab(T_a-T_b)\alpha(1+2\lambda)}{2(a-b)}$.